Composites Science and Technology 211 (2021) 108871

Contents lists available at ScienceDirect

Composites Science and Technology

journal homepage: www.elsevier.com/locate/compscitech

Transient deformation and curvature evolution during the snap-through of a bistable laminate under asymmetric point load

Vishrut Deshpande *, Oliver Myers, Georges Fadel, Suyi Li

Department of Mechanical Engineering, Clemson University, Clemson, SC, USA

ARTICLE INFO

Keywords:
Bistable laminate
Snap-through
Asymmetric load

ABSTRACT

Bistable carbon fiber composites, whose bistability arises from having asymmetric fiber layouts in different layers, have shown immense potential for using in shape morphing and adaptive structure applications. While many studies in this field focus on these composite laminates' external shapes at the two stable states, their snap-through behavior of shifting from one stable shape to the other remains a critical aspect to be investigated in complete detail. Moreover, symmetric loading conditions have been extensively studied based on the classical lamination theory, but the asymmetric loading conditions received far less attention. Therefore, this study examines an asymmetric, localized point load on a [0°/90°] bistable laminate and its complex transient deformation during the snap-through. Finite element simulation and experiment results reveal three uniquely different snap-through behaviors — two-step snap, one-step snap, and no snap — depending on the point load location. The localized initiation and propagation of a "curvature inversion zone," calculated from finite element and digital image correlation results, are directly related to these snap-through characteristics. This study also explored the feasibility of using an extended analytical model of classical lamination theory to qualitatively reproduce the above findings. This model compares three polynomial functions of different orders to approximate the out-of-plane laminate displacement field. This study's results can offer valuable insights into the fundamental mechanics of snap-through behaviors and the actuation designs for the bistable composites for different loading scenarios.

1. Introduction

With a continuously evolving engineering technology, our need for next-generation structures and materials with novel functionalities has increased significantly. To this end, we have witnessed the development of many "smart" structures that exploit the nonlinear phenomenon of *bistability* — the co-existence of two distant stable equilibria. A bistable structure can settle into either of its stable equilibria (or stable states) without external aid. However, if an external or internal actuation deforms such a structure to a critical configuration, elastic instability would occur and rapidly switch the structure to a different stable state; this process is referred to as the *snap-through*. The applications of bistable structures span across mechanical [1,2], electronic [3,4], and biochemical systems [5,6]. In particular, there has been a surge of interest in integrating the bistability in meta-materials [7–9], robotics [10–12], origami structures [13–15] and energy harvesters [16,17], which are amongst the emerging engineering technologies.

One promising example of bistable structures is the *asymmetric* Carbon Fibre Reinforced Polymers (CFRPs), pioneered in Hyer and Dano's groundbreaking study in 1981 [18]. The reinforcing fibers in these structures are oriented differently in each layer, and their order is non-symmetric through the thickness direction (e.g., [0°/90°] layup in Fig. 1 (a)). As a result, bi-stability occurs due to the non-uniform residual stress developed in the curing process. These asymmetric composites can feature a higher strength to weight ratio and better conformability than other types of bistable structures, and many applications have seen benefits from utilizing them, such as automobiles [19], morphing airframes, and wind turbine blades [20–22]. Potential applications also extend in renewable energy infrastructure [22–24], and energy harvesting [25].

The promising potentials of these bistable composites sparked many research efforts, and an important question is to predict the composite's external shapes at different stable states theoretically. Hyer and Dano formulated a model using classical lamination theory in an early work [26], and they used cubic polynomials to approximate the strain fields and quadratic polynomials for the out-of-plane displacements of a

* Corresponding author.
E-mail address: vdeshpa@clemson.edu (V. Deshpande).

https://doi.org/10.1016/j.compscitech.2021.108871
Received 19 November 2020; Received in revised form 10 May 2021; Accepted 15 May 2021
Available online 21 May 2021

simple [0°/90°] laminate. As the curvatures are second-order derivatives of the out-of-plane displacements, this model predicted cylindrical-shaped composite laminate with a uniform curvature distribution. However, it also over-predicted the deformations for cross-ply laminates with more generic [$\theta/\theta-90°$] ply layouts. In a more recent study, Weaver et al. presented a different method for estimating the laminate's curvature, which correlated the neutral planes of fiber plies to their anisotropic elastic moduli, and assumed linear strain distribution through the thickness [27]. By minimizing the total potential energy with respect to curvature, this model calculated the laminate's maximum deflection at a stable state with a satisfactory agreement with the experimental measurements. Examinations of the external shapes continue to evolve, with new analytical methods [28,29], the inclusion of embedded actuators like piezoelectric patches [28,30–32], and extension to multi-patched structures [21,33–35].

Besides the external shapes, the asymmetric composites' snap-through deformation as they switch between the stable states also received attention. Dano et al. examined snap-through by using weights to apply symmetric bending moments from the opposite edges of a bistable laminate [36]. To predict the critical load required for snap-through, they also revised their mathematical model by including the virtual principle and approximating the strain field using quadratic polynomials rather than cubic. The predicted loads (moments) for snap-through showed good agreement with the experiment results. Cantera et al. captured the load-displacement curves and intermediate laminate shapes during snap-through and snap-back, where the square laminates of varying side lengths were held at corners and loaded at the center [37]. Potter et al. provided another critical insight regarding the bifurcations during the snap-through of [0°/90°] laminate [27]. They found that the snap-through occurs via two closely coupled bifurcations rather than a single bifurcation. However, they did not examine the nature of these two bifurcations in detail. Pirrera et al. compared the performance of higher-order polynomials in predicting the snap-through behaviors [29]. Their experiment involved four loads at the corners of a freely supported square laminate to measure the force-displacement relationship during snap-through. They then attempted to theoretically reproduce the experiment results by approximating the laminate deformation using different polynomials functions, and concluded that the polynomials had to be of a high order (eleventh in their study) to produce a quantitative agreement with the FEA result.

All the studies of snap-through deformations mentioned above, however, only involved symmetric loading to the laminate. Moreover, several studies pointed out the importance of curvature change during the snap-through [27,29], but none of them examined its role in detail. Therefore, the objective of this paper is to 1) examine the transient snap-through deformations of bistable composite laminate under *asymmetric* and *localized* point load, and 2) investigate the role of curvature changes. More specifically, we fix a [0°/90°] square laminate at its center and apply a transverse point load at different locations (either along the laminate edge or in the interior). We measure the force-displacement relationships corresponding to different loading positions during snap-through and used the digital image correlation (DIC) technique to track the laminate deformation and surface curvature evolution in real-time. Finite element simulation is carried out in parallel to cross-validate the experimental observations. Our results show that, as we change the loading positions, the bistable laminate exhibits three uniquely different snap-through behaviors even though its external shapes before and after snap-through remain the same. That is, depending on its position, the point load can either complete the snap-through with two consecutive steps or one step. However, at some locations, the point load cannot induce a snap-through at all. The localized distribution and propagation of curvature changes (or curvature inversions) are directly related to these unique snap-through behaviors. Moreover, to assess the feasibility of theoretically predicting these complex deformations, we conduct a comparative study based on an extension of Hyer's model with three different polynomial functions that approximate the laminate deformation. Our results show that a higher-order polynomial is necessary to reproduce the experiment and finite element results qualitatively, but there are trade-offs and limitations.

Since the bistable composites are increasingly popular in systems that involve dynamic loading conditions (e.g., morphing applications), it is crucial to understand their deformation characteristics under complex external stimuli. On the most fundamental level, this study establishes the behavioral trends and requirements for completing the snap-through between two stable states. Therefore, our results on the [0°/90°] bistable laminate under localized load can provide a comprehensive insight and actuation design guidelines for many upcoming applications.

In what follows, Section 2 first explains the experiment and finite element setup, and then details the unique snap-through behaviors corresponding to different point load locations. Section 3 presents the comparative study using the extended analytical model. Section 4 concludes this paper with a summary and discussion.

2. Observations on snap-through and curvature evolution

2.1. Methods and materials

The bistable composite laminate samples in this study are 100 × 100

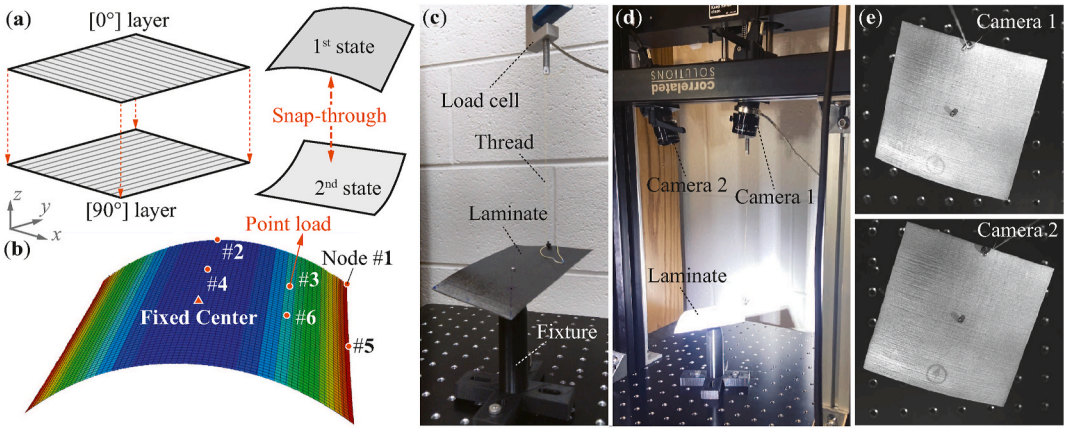

Fig. 1. The experimental and finite element simulation setup of this study. (a) The square-shaped bistable composite laminates consist of two fiber prepregs with a [0°/90°] layout. (b) Finite element simulation result showing the shape of first stable state, the mesh size, the fixed center, and the six nodes selected for localized point loading. (c) The experimental apparatus for measuring the reaction force-displacement relationships. (d) The experiment setup fitted with Digital Image Correlation (DIC) equipment. (e) Two example images from the two cameras, highlighting the two different angles and manually sprayed speckled laminate.

mm in size, made from DA409u 8552 unidirectional carbon fiber prepregs having ply thickness of 0.15 *mm*. A layer of 0° prepreg was placed on top of a 90° layer to develop the asymmetric [0°/90°] layout (Fig. 1 (a)), and then cured the assembly in an oven at 135°C to develop bistability. Vacuum bagging techniques were used in the fabrication, and interested readers can refer to the authors' previous publication for more details [38]. Table 1 summarizes the constituent material properties of the prepregs.

To measure the reaction force-deformation of the bistable patch under localized load, a small hole was drilled at the center of a bistable laminate and fixed it to a 3D-printed fixture with a bolt. This fixture has a tall tower with the laminate on its top, and four legs with adjustable screw holes for mounting on a universal testing machine (ADMET eXpert 5061) (Fig. 1(c)). This test setup fully constraints the translational and rotational motions at the laminate center. To apply a localized load, an eyebolt was fastened at the selected node on the laminate, and connected it to the universal tester's moving overhead with a nylon thread. This thread was changed for every run and was ensured to be taught before the start of snap-through experiment to minimise any slackness errors or length variation errors. A controlled overhead displacement of (0.5 mm/s) is applied at the selected node until snap-through completes, and the load cell (ADMET eXpert S-type 500 series) records the corresponding reaction force.

Besides measuring the reaction force-deformation relationship, the digital image correlation (DIC) was used to track the transient patch deformation throughout the snap-through process (Fig. 1(d and e)). The DIC test involves two high-speed cameras that focus from top of the testing machine, adjusted to an optimum height in order to capture the 3D displacement field of the complete laminate accurately. The camera frame rate was set at 30 fps, which turned out to be sufficient to capture the rapid composite deformation in snap-through. The nodal coordinates are extracted from the DIC data by Vic3D software (Correlated Solutions) to calculate the distribution of surface mean curvatures at different stages of loading.

The setup of finite element simulation (ABAQUS 6.14, Static Structural Solver) is the same as the experiment regarding the fiber laminate design, constituent material properties, boundary conditions, and localized loading. The laminate is modeled using the standard *S4R* elements with a mesh density of 41×41 nodal points. The simulation involves two consecutive steps: The first step cures the laminate from its initially flat configuration to a stable state. The second step snaps the laminate to another stable state by applying sufficient displacement at the selected node, one at a time.

During the first curing step, the laminate is fixed completely flat, as in the vacuum bagging techniques [38]. Then, we applied simulated heating at 135° C and cooling to room temperature at 20° C, allowing internal thermal stress to develop. Once cured, the laminate is released from its fixed condition and free to deform into one of the two stable shapes. In the second snapping step, the laminate is constrained at its center, as shown in Fig. 1(b). The middle node is fixed in the $x-y$ reference plane with no rotation allowed about the z-axis (i.e, $U1$, $U2$, $UR3 = 0$). The four nodes adjacent to the middle node are constrained in the z-axis ($U3 = 0$). Then, we simulate a controlled displacement at the selected node until snap-through completes. The simulation records the reaction forces in all three directions ($RF1$, $RF2$, $RF3$) and displacements ($U1$, $U2$, $U3$) at the selected node of loading, and then calculate the total reaction force-nodal displacement relationship.

Table 1
Constituent material properties of DA409u 8552 carbon composite prepregs. E_i and G_{ij} are the elastic modulus (unit of GPa). ν is the Poisson's ratio. α_{ij} are the thermal coefficients of expansion (unit of $°C^{-1}$).

Property	Value	Property	Value	Property	Value
E_1	135	G_{12}	5	α_{11}	-2×10^{-08}
E_2	9.5	G_{13}	7.17	α_{22}	3×10^{-05}
ν_{12}	0.3	G_{23}	3.97	α_{33}	3×10^{-05}

In this study, we focus on three different responses to examine the transient snap-through behaviors of the bistable laminate under asymmetric point load. They are the intermediate deformation, change in curvature distribution, and the reaction force during the snap-through. We discovered that as we move the point load location, the transient behavior of the composite laminate fundamentally changes *during* the snap-through irrespective of its two stable states *before and after*. The subsections below discuss three representative cases in detail.

2.1.1. Point load at laminate corner (node #1)

When the point force is at node #1 (defined in Fig. 1(b)), snap-through occurs in two consecutive steps, as indicated by the two sharp drops in the force-displacement curves in Fig. 2(a). The variation in the experimental response curves attributes to three different samples being tested, the unavoidable errors in the fabrication process, and discrepancy in the fixture holding torque. By carefully observing the patch deformation both in the experiment and finite element simulations (Fig. 2(b)), we find that the first step occurs when the initially straight edge of the laminate (right edge in Fig. 2(b)) acquires a curved shape. This relatively rapid change in the edge shape explains the first peak and then dip in the force-displacement curve and marks the onset of shifting from one state to the other. The second step occurs when the top, initially curved edge of the laminate becomes straight. It is worth noting that if we remove the point load before the second snap occurs, the laminate would return to its original stable state. On the other hand, after the second step occurs, the laminate would settle into a new stable state if the point load is removed.

Besides the reaction force, we further examine these transient snap-through behaviors based on the distribution of mean curvature in the bistable laminate. Fig. 2(c) and the supplemental video illustrates the evolution of curvature distribution throughout the snap-through based on finite element simulation and the DIC measurements. Before loading, the curvature of the fiber laminate is relatively uniform and negative. This is consistent from the findings of Portela et al. and reassures are results [32]. When the point load starts, we observe a region of inverted (positive) curvature that starts to initiate and grow from the loading point and the fixed center. we refer to this region as "curvature inversion zone" hereafter. As the node #1 displacement increases, the front of this curvature inversion — which corresponds to the front of zero mean curvature — begins to propagate. More importantly, when the curvature inversion reaches the bottom edge of the bistable laminate, the first step of the snap-through completes (iii). As the node #1 displacement continues to increase, the curvature inversion zone progresses slowly along the top edge to the left. When it finally reaches the left edge, the second snap occurs and laminate rapidly deforms to the new stable state with a relatively uniform distribution of positive curvature.

It is worth noting that the experiment results agree with finite element simulation reasonably well (regarding both the reaction force from the universal tester in Fig. 2(a) and the curvature measurement from DIC in Fig. 2(c)). Differences in the experimental results and FEA simulations are due to the fact that the material properties of the prototype might differ slightly from those used in the simulation. And the manual fabrication error also plays a role. Based on the simulation, the critical force required for the snap-through is 0.70 N (maximum reaction force), and the critical displacement is 29.0 mm (at the occurrence of the second step).

2.1.2. Point load at the mid-point of initially curve edge (node #2)

If the point load moves to the mid-point of initially curved edge (node #2 in Fig. 1(b)), the bistable laminate snap-through occurs in only one step. During the snap-through, the initially curved edge at which node #2 is located and the adjacent straight edges (right and left edges) change their shapes simultaneously. That is, the initially curved top edge becomes straight and initially straight left/right edges becomes curved

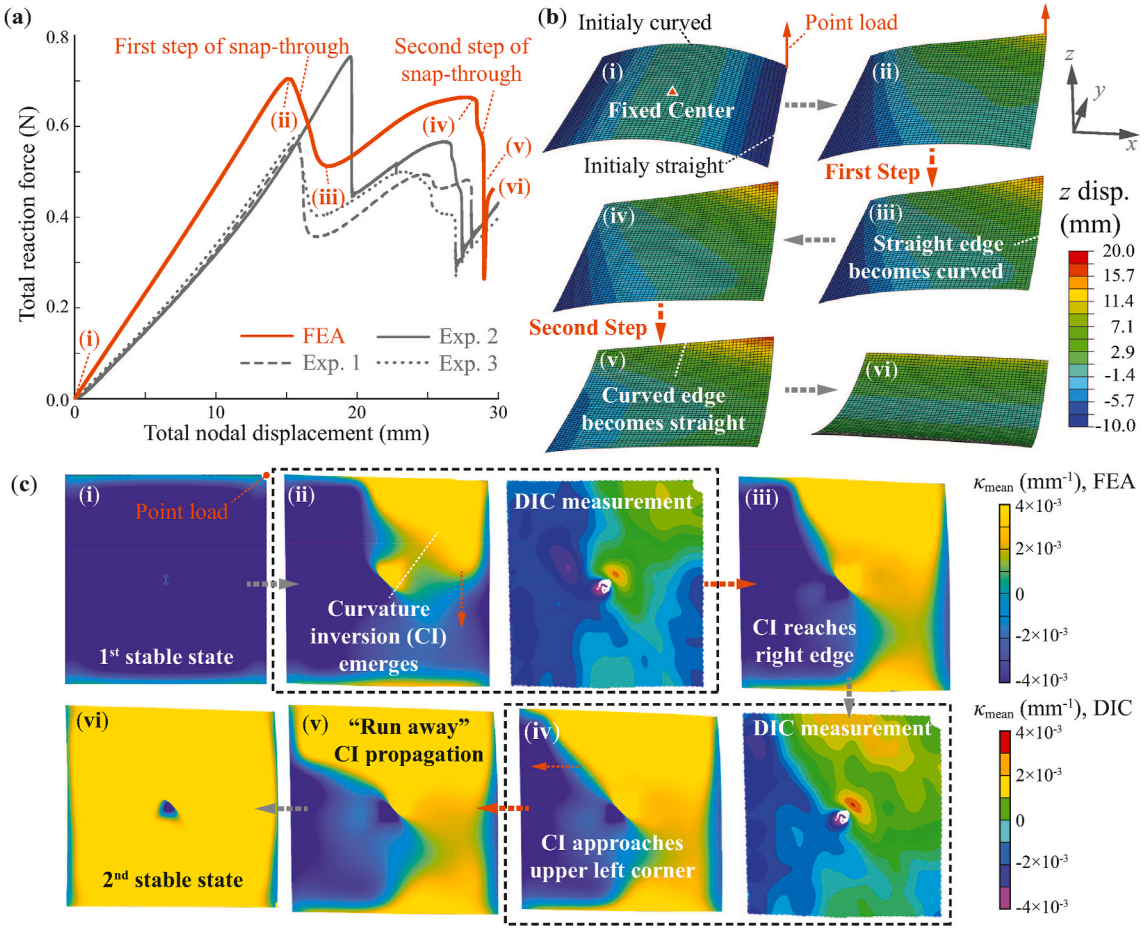

Fig. 2. The transient deformation during the snap-through when the point load is at the corner (Node #1). Different instants throughout this process are labeled from (i) to (vi). (a) The reaction force-deformation relationship from finite element simulations and experiments. (b) Finite element simulations show the progressive switches regarding the shape of the different laminate edges. (c) The mean curvature distribution shows a complicated evolution during the snap-through. These curvature results come from finite element simulation.

at the same time. Therefore, the deformation occurs almost symmetrically about the longitudinal axis passing through the fixed center, as shown in Fig. 3(b)). Such symmetry in snap-through is also evident in the distribution of mean curvature (Fig. 3(c) and supplemental video). We observe that the fronts of curvature inversion zone progress symmetrically towards the top edge. When these fronts reach the respective right and left edges, snap-through occurs, and the laminate deforms to the new stable state rapidly. The corresponding critical force required for completing the snap-through is 4.1 N based on finite element, and the corresponding critical displacement is 16.7 mm.

2.1.3. *Point load at the mid-point of initially straight edge (node #5)*

If the point load is at the mid-point of the initially straight edge (node #5 in Fig. 1(b)), snap-through never occurs regardless of the load amplitude (Fig. 4). This unique observation has never been reported by previous studies. By carefully observing the evolution of curvature distribution (Fig. 4(c) and supplemental video), we discover that the curvature inversion zone never fully reaches the initially straight edge where the point force locates, even though the inversion zone can reach the initially curved edge (top and bottom edge in Fig. 4(c)).

2.1.4. *Point load at other positions*

When the point load is at node #3, snap-through also occurs in two steps. After a careful observation of the finite element simulation and experiment result, we found that the transient deformation and curvature development are similar to those of node #1. However, unlike the case for node #1, the distance between these two steps in terms of point load displacement is minimal (Fig. 5 shows the zoom-in view at the point of snap). When node #4 is under point load, the transient deformation is similar to that of node #2. That is, the snap-through occurs in only one step. However, the critical force requirement for snap-through increases significantly, whereas the critical displacement reduces. These differences indicate that the laminate gives more resistance as the point load moves closer to the fixed center. The curvature inversion development is similar to the node #2 case in that two inversion fronts originate from the center and progress towards the top and right edges. Finally, if the point load is at node #6, snap-through never occurs regardless of the load amplitude. For clarity, the critical force and displacement corresponding to the six different point load locations are summarized in Table 2.

Therefore, we deduce that if the loading point is on the axis defined by node #2 and laminate center, the corresponding snap-through involves only one step. Also, there would be two fronts of curvature inversion emerging out of the laminate centre and progressing towards respective left and right edges, thus snap-through happens symmetrically. If the point load is on the axis defined by node #5 and laminate center, no snap-through will occur. Thus, a full curvature inversion never occurs. Otherwise, the snap-through involves two steps and a single front of curvature inversion develops and progresses through the laminate asymmetrically. Moreover, we deduce that the snap-through is complete only when the curvature inversion zone reaches *both* of the initially straight edges. In the following subsection, we use the analytical model to test these observations.

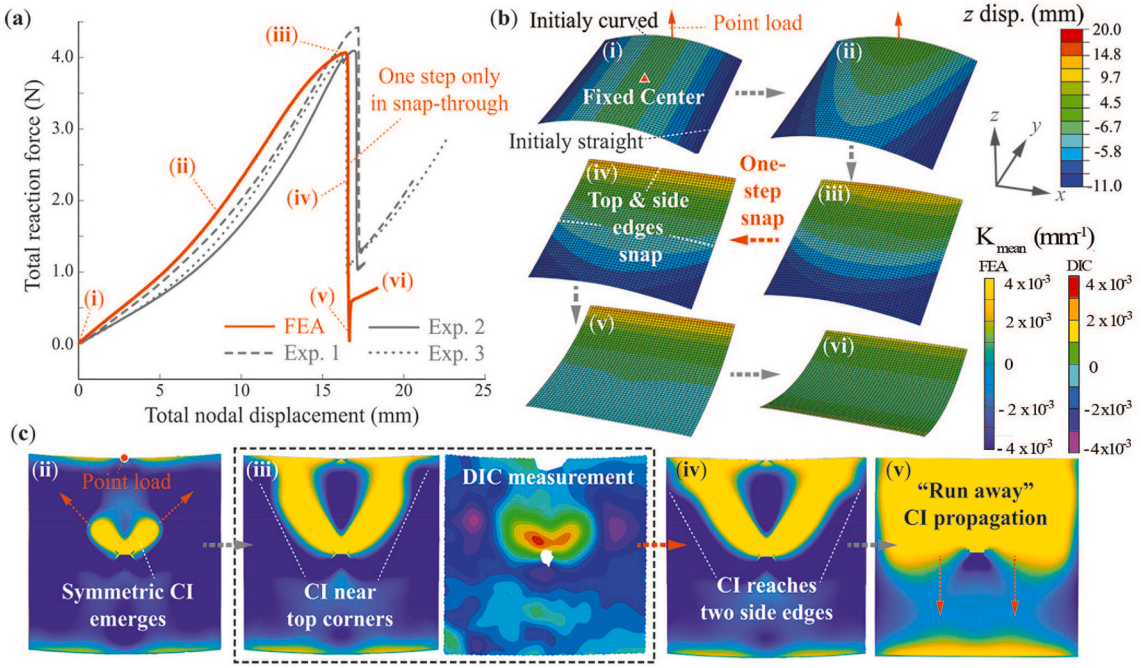

Fig. 3. The transient deformation during the snap-through when the point load is at the center of initially curved edge (Node #2). Different instants throughout this process are labeled from (i) to (vi) (a) The reaction force-deformation relationships show that, in this case, the snap-through consists of only one step. (b) Finite element simulations show the simultaneous switches regarding the shape of the different laminate edges. (c) The mean curvature distribution shows a symmetric evolution during the snap-through. At the beginning of snap-through (labeled by iii, iv), we also included the mean curvature based on DIC readings for validation. Here, the curvature distribution at the first stable state (i) and second stable state (vi) are omitted since they are the same as those in Fig. 2(c).

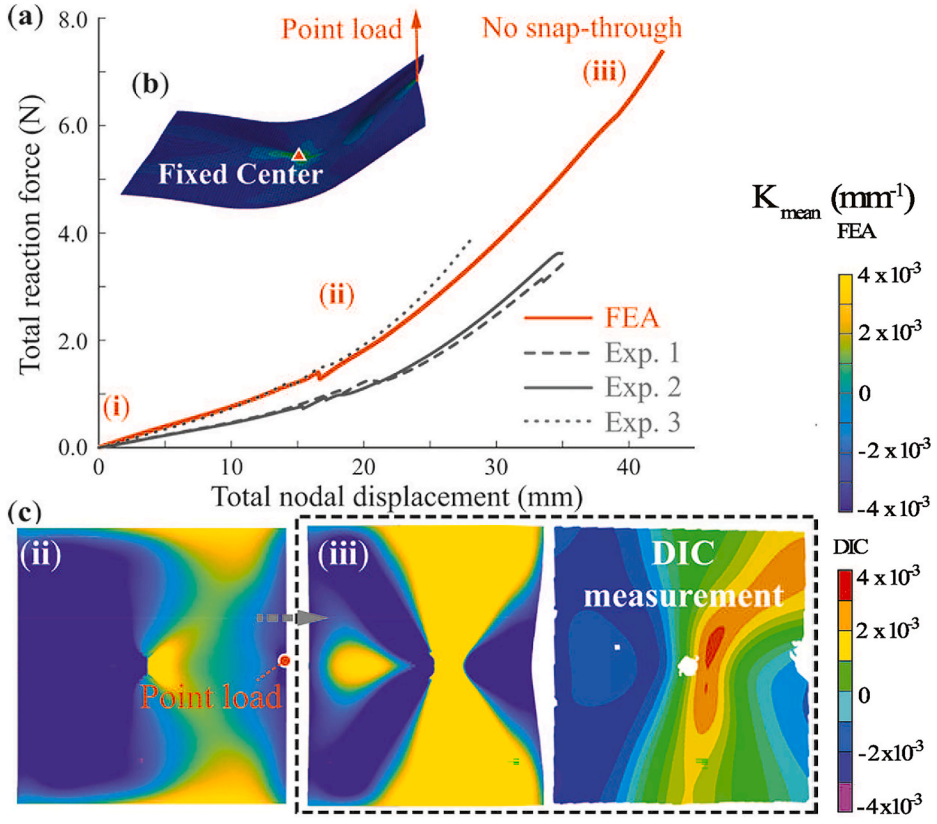

Fig. 4. The transient deformation during the snap-through when the point load is at the center of initially straight edge (Node #5). (a) The reaction force-deformation relationships show that, in this case, no snap-through occurs. (b) Finite element simulations showing the deformed shape of the laminate. (c) The mean curvature distribution based on finite element and DIC data.

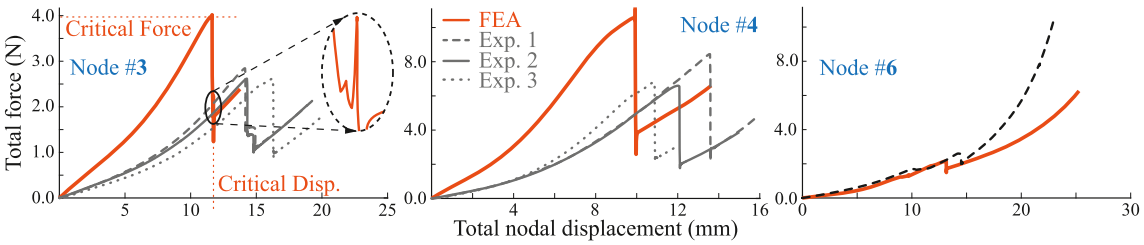

Fig. 5. The force-displacement relationships based on other loading positions. At node #3, the snap-through involves two steps, although the distance between the two steps are very small. At node #4, snap-through involves only one step. At node #6, no snap-through occurs.

Table 2
Critical Displacement and Reaction forces for point loading at different nodes.

Node	Method	Critical Force	Critical Displacement
1	Simulation	0.70N	29.0 mm
	Experiments	0.63N ± 14.3%	27.4 mm ± 1.5%
	% difference	12.8%	5.5%
2	Simulation	4.07N	16.7 mm
	Experiments	4.19N ± 3.8%	17.0 mm ± 1.8%
	% difference	2.9%	1.7%
3	Simulation	3.97N	11.7 mm
	Experiments	2.68N ± 4.5%	15.4 mm ± 4.5%
	% difference	32.4%	31.6%
4	Simulation	10.56N	9.9 mm
	Experiments	7.24N ± 11.7%	12.2 mm ± 9%
	% difference	31.4%	23.2%

3. Analytical investigation using an extended Hyer's model

To approximate the shape and curvature changes during the snap-through of the laminate and recreate the observations from above, we formulated a comprehensive analytical model by extending the Hyer's model, a widely used method for analyzing bistable composite laminates [21,25,33,36]. This model's accuracy and capability hinge on the order of polynomial functions that approximate the laminate's deformation. Hyer and Dano chose a second-order polynomial for the out-of-plane displacement field. Hence the curvatures of the composite laminate were constant and uniform [18]. Mattioni used a product of two parabolic equations in both x and $y-$ directions [33]. As a result, the corresponding curvature distribution was a reduced second-order polynomial.

However, the Hyer's model and its variations are mostly used for predicting the external shape *at* the stable states, few used this model to estimate the transient deformation *between* stable states, let alone the asymmetric loading in this study. Therefore, we want to explore the feasibility of using the extension of Hyer's model — by comparing the results from third, fourth, and fifth-order polynomials functions — for new insights.

From the Hyer's model, the total strain energy of the bistable laminate is formulated using the following equation

$$\Pi = \int_{-L_x/2}^{L_x/2}\int_{-L_y/2}^{L_y/2} \frac{1}{2}\begin{bmatrix}\varepsilon_0 & \kappa\end{bmatrix}\begin{bmatrix}A & B\\ B & D\end{bmatrix}\begin{bmatrix}\varepsilon_0\\ \kappa\end{bmatrix} - \begin{bmatrix}\varepsilon_0 & \kappa\end{bmatrix}\begin{bmatrix}N_t\\ M_t\end{bmatrix} \mathrm{d}y\,\mathrm{d}x, \tag{1}$$

where the mid-plane strains ε_0 and curvatures κ of the laminates are

$$\varepsilon_0 = \begin{bmatrix}\varepsilon_{x0}\\ \varepsilon_{y0}\\ \gamma_{xy0}\end{bmatrix}; \quad \kappa = \begin{bmatrix}\kappa_x\\ \kappa_y\\ \kappa_{xy}\end{bmatrix} = \begin{bmatrix}-\dfrac{\partial^2 W_0}{dx^2}\\ -\dfrac{\partial^2 W_0}{\partial y^2}\\ -2\dfrac{\partial^2 W_0}{\partial x \partial y}\end{bmatrix}. \tag{2}$$

In Equation (1), different terms in the "stiffness" matrices are

$$A_{ij} = \sum_{k=1}^{k=n} \overline{Q}_{ij}^{(k)}\left(z_k - z_{k-1}\right); B_{ij} = \frac{1}{2}\sum_{k=1}^{k=n} \overline{Q}_{ij}^{(k)}\left(z_k^2 - z_{k-1}^2\right); D_{ij} = \frac{1}{3}\sum_{k=1}^{k=n} \overline{Q}_{ij}^{(k)}\left(z_k^3 - z_{k-1}^3\right) \tag{3}$$

where the index k represents the different layers in the laminate (in this study, $k = 1, 2$). The in-plane thermal resultant forces (N_t) and moments (M_t) induced by the curing are,

$$N_t = \sum_{k=1}^{k=n} \overline{Q}_{ij}^{(k)}\alpha_t \nabla T\left(z_k - z_{k-1}\right); \; M_t = \frac{1}{2}\sum_{k=1}^{k=n} \overline{Q}_{ij}^{(k)}\alpha_t \nabla T\left(z_k^2 - z_{k-1}^2\right). \tag{4}$$

The vector of thermal expansion coefficient is expressed as $\alpha_t = [\alpha_x\ \alpha_y\ \alpha_{xy}]^\intercal$. In the above Equations (3) and (4), $\overline{Q}^{(k)}$ is the stiffness of the k^{th} fiber prepreg layer, transformed from the material coordinate system to the geometry coordinate system. The matrix Q in the material coordinate system is

$$Q = \begin{bmatrix}\dfrac{E_1}{1-\nu_{12}\nu_{21}} & \dfrac{\nu_{12}E_2}{1-\nu_{12}\nu_{21}} & 0\\ \dfrac{\nu_{12}E_2}{1-\nu_{12}\nu_{21}} & \dfrac{E_2}{1-\nu_{12}\nu_{21}} & 0\\ 0 & 0 & G_{12}\end{bmatrix} \tag{5}$$

From Q, on can calculate $\overline{Q}$ of every layer in that $\overline{Q}^{(k)} = T^{-1}Q^{(k)}T^{-\intercal}$, where the transformation matrix T is

$$T = \begin{bmatrix}\cos^2\theta & \sin^2\theta & \sin 2\theta\\ \sin^2\theta & \cos^2\theta & -\sin 2\theta\\ -\sin\theta\cos\theta & \sin\theta\cos\theta & \cos 2\theta\end{bmatrix}. \tag{6}$$

The most critical part of this analytical approach is the estimation of strains, curvatures, and hence the displacements of the bistable composites. The in-plane tensile strains are estimated using complete second order polynomials in that

$$\begin{aligned}\varepsilon_{x0} &= c_1 + c_2\frac{x}{L_x} + c_3\frac{y}{L_y} + c_4\frac{x^2}{L_x^2} + c_5\frac{y^2}{L_y^2} + c_6\frac{xy}{L_xL_y},\\ \varepsilon_{y0} &= c_7 + c_8\frac{x}{L_x} + c_9\frac{y}{L_y} + c_{10}\frac{x^2}{L_x^2} + c_{11}\frac{y^2}{L_y^2} + c_{12}\frac{xy}{L_xL_y},\end{aligned} \tag{7}$$

where c_i are constants to be determined. It is worth highlighting that, unlike the previous studies [18,33], the linear terms in the strain estimation must be included. They were considered insignificant and thus omitted previously. However, these terms' influences are significant in this study due to the localized deformation in the laminate. Moreover, we normalize every term in the polynomials, i.e. divide by the laminate's size in either x or $y-$ dimension with the same power as that particular term. This normalization can increase the computational efficiency of numerical solver.

We estimate the out-of-plane displacement field of the laminate (in $z-$ axis) using complete third-order, fourth-order, and fifth-order polynomial functions. Accordingly, the assumed curvatures (which are

second-order differentials of out-of-plane displacement) are linear, second-order, and third-order polynomials. The $z-$ displacement polynomials are listed below,

$$W_0 = c_{13}\frac{x^2}{L_x^2} + c_{14}\frac{y^2}{L_y^2} + c_{15}\frac{xy}{L_xL_y} + c_{16}\frac{x^2y}{L_x^2L_y} + c_{17}\frac{xy^2}{L_xL_y^2} + c_{18}\frac{x^3}{L_x^3} + c_{19}\frac{y^3}{L_y^3}, \tag{8}$$

$$\begin{aligned} W_0 = {} & c_{13}\frac{x^2}{L_x^2} + c_{14}\frac{y^2}{L_y^2} + c_{15}\frac{xy}{L_xL_y} + c_{16}\frac{x^2y}{L_x^2L_y} + c_{17}\frac{xy^2}{L_xL_y^2} + c_{18}\frac{x^3}{L_x^3} \\ & + c_{19}\frac{y^3}{L_y^3} + c_{20}\frac{x^2y^2}{L_x^2L_y^2} + c_{21}\frac{x^3y}{L_x^3L_y} + c_{22}\frac{xy^3}{L_xL_y^3} + c_{23}\frac{x^4}{L_x^4} + c_{24}\frac{y^4}{L_y^4}, \end{aligned} \tag{9}$$

$$\begin{aligned} W_0 = {} & c_{13}\frac{x^2}{L_x^2} + c_{14}\frac{y^2}{L_y^2} + c_{15}\frac{xy}{L_xL_y} + c_{16}\frac{x^2y}{L_x^2L_y} + c_{17}\frac{xy^2}{L_xL_y^2} + c_{18}\frac{x^3}{L_x^3} + c_{19}\frac{y^3}{L_y^3} \\ & + c_{20}\frac{x^2y^2}{L_x^2L_y^2} + c_{21}\frac{x^3y}{L_x^3L_y} + c_{22}\frac{xy^3}{L_xL_y^3} + c_{23}\frac{x^4}{L_x^4} + c_{24}\frac{y^4}{L_y^4} + c_{25}\frac{x^2y^3}{L_x^2L_y^3} + c_{26}\frac{x^3y^2}{L_x^3L_y^2} \\ & + c_{27}\frac{x^4y}{L_x^4L_y} + c_{28}\frac{xy^4}{L_xL_y^4} + c_{29}\frac{x^5}{L_x^5} + c_{30}\frac{y^5}{L_y^5}. \end{aligned} \tag{10}$$

The in-plane displacements of the laminate (U_0, V_0) are determined by using the strain formulations,

$$U_0 = \int\left[\varepsilon_{x0} - \frac{1}{2}\left(\frac{\partial W_0}{\partial x}\right)^2\right]\mathrm{d}x + g(y)\ ;\ V_0 = \int\left[\varepsilon_{y0} - \frac{1}{2}\left(\frac{\partial W_0}{\partial y}\right)^2\right]\mathrm{d}y + h(x). \tag{11}$$

Here, $g(y)$ and $h(x)$ serve to complete the in-plane displacements and eliminate the rigid-body rotations:

$$g(y) = g_1\frac{y}{L_y} + g_2\frac{y^3}{L_y^3} + g_3\frac{y^5}{L_y^5}\ ;\ h(x) = h_1\frac{x}{L_x} + h_2\frac{x^3}{L_x^3} + h_3\frac{x^5}{L_x^5}. \tag{12}$$

To make sure the rigid body rotation is eliminated, g_1 has to equal to h_1. Finally, the in-plane shear strain is

$$\gamma_{xy0} = \frac{\partial U_0}{\partial y} + \frac{\partial V_0}{\partial x} + \frac{\partial W_0}{\partial x}\frac{\partial W_0}{\partial y}. \tag{13}$$

The analytical model has twelve undetermined constants from the strain estimations, five from the in-plane displacement estimations, and more from the out-of-plane displacement estimation (W_0) depending on the order of the polynomials. The total number of undetermined constants for third-order polynomial is 24, for fourth-order polynomial its 29, and fifth-order polynomial it is 35.

Here, we obtain the solution by minimizing the strain energy (Eq. (1)) using the MATLAB `fmincon` function, which is a constrained multivariable optimizer for highly non-linear problems. To reduce the computational time, we used the "interior-point" algorithm and explicitly derived the gradients of strain energy with respect to the undetermined constants.

Like the experiment and finite element, solving the analytical model involves two steps: curing and snapping. In the first step, we use the same temperature (i.e., $\nabla T = 20^{\circ}C - 135^{\circ}C$) to calculate the laminate shape right after curing. Moreover, no constraints are enforced in this step so that the undetermined constants can take any real values. In the second step of snapping the laminate from one stable state to another, we apply the localized loading (controlled displacement) by using the equality constraints from `fmincon` in a novel way. Denote $x = x_{load}$ and $y = y_{load}$ as the loading position and $d_{initial}$ as the calculated out-of-plane displacement of this position after the first curing step, we assign an equality constraint during optimization in that

$$W_0(x = x_{load}, y = y_{load}) = d_{initial} + \delta d, \tag{14}$$

where δd is the increment displacement loading. We increase δd until the laminate shifts to the other state. In this way, we can observe the laminate's intermediate shapes during loading and calculate the strain energy corresponding to every δd increment. This could be understood as way of solving the problem using a quasi-static approach, in which every intermediate step is calculated to quasi-stable shape by minimizing the potential function of the laminate when it is held at that increment displacement loading. Now, the reaction force becomes

$$F = -\frac{\mathrm{d}\Pi}{\mathrm{d}(\delta d)}. \tag{15}$$

As we have three different polynomials to estimate the out-of-plane displacement field, we derive results from all of them for each case.

3.1. Two-step snap at node #1

Fig. 6 summarizes the analytical prediction when the point load is at Node #1. We observe that the third-order polynomial estimation (aka. linear mean curvature distribution) gives a clear indication that the snap-through process involves two different steps (Fig. 6(a)). The response curve from the fourth order polynomial — although also conveys that the overall snap-through has two-step — does not match experimental or FEA results well. The fifth order polynomial results (aka. cubic distribution of mean curvatures) successfully capture the trend qualitatively when compared to FEA and experimental results. We see that the reaction force increases and reaches its critical force at point (ii), where the initially straight edge at the right deforms into a curved shape ((ii)-(iii) in Fig. 6(b)). Then the reaction force decreases to a local minimum and increases again, a trend similar to finite element and experiment results. The increase in the reaction force from this local minima is relatively gradual and, at the critical displacement, the laminate snaps completely to its second stable state in that the top edge changes from a curved shape to straight. Moreover, the reaction force at the occurrence of second step ((v) in Fig. 6(a)) is less than the critical force at point (ii). This phenomenon of right edge snapping first and then top edge (hence the lag between two peaks) is captured satisfactorily by the fifth order polynomial model and correlates well to the FEA and experiment results. Here, its worth noting that some modifications were found necessary in-order to get the correct results. That is, c_2, c_5, c_9, and c_{10} are set to zero. The physical principle underpinning this modification will be the subject of future study.

The fifth order polynomial approximation of the out-of-plane displacement give a cubic distribution of mean curvature, which gives a fair representation of the curvature inversion (CI) evolution (Fig. 6(c)). We observe that the CI front develops at the top corner point where the load is applied and then progresses throughout the laminate. It reaches the bottom edge first, snapping the right edge to deformed curve shape. Then it progresses towards the top left corner. At the critical configuration (Fig. 6(c)(v)), the curvature inversion reaches the left edge and hence, the laminate snaps rapidly to a new stable state.

3.2. No-snap at node #5

Similar to what we observe from the FEA and experimental results, the laminate does not snap if the load is applied at node #5 in the analytical model. This is true for all of the three polynomial estimations for out-of-plane displacement field. Fig. 7(b) shows the sequence of intermediate shapes of laminate during the point load application. We observe that the right edge changes to a curved shape for a short while but quickly shifts back straight, indicated by the small dip in the force-reaction curve. This phenomenon was also observed in the experiment.

Similar to the curvature results we obtained from FEA and DIC, curvature inversion does not occur completely in the laminate. We observe that the initial negative curvature of the laminate starts to invert from the centre towards the opposite top and bottom edges. And then slowly progresses in the laminate but never reaches the right or left edges. This is the reason due to which the laminate never snaps.

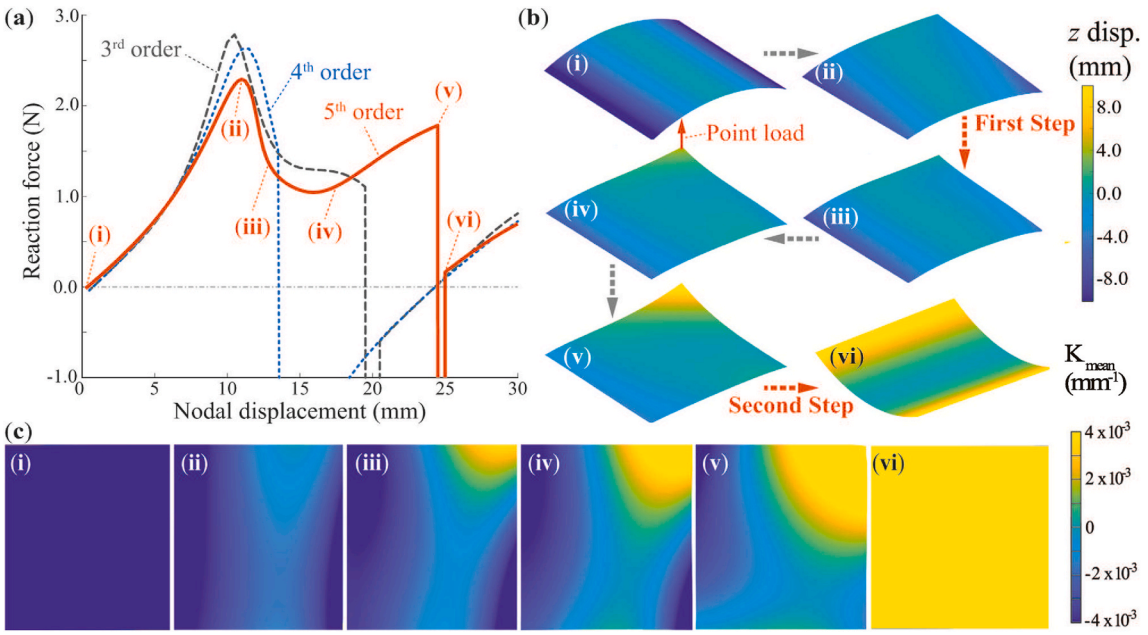

Fig. 6. Analytical prediction of the transient deformation during the snap-through when the point load is at the corner (Node #1). (a) The reaction force-deformation relationships based on three polynomial functions with different orders. (b) Simulated patch deformation based on the fifth order polynomial fit. (c) The mean curvature distribution based on fifth order polynomial fit. The colormap in this case is the same as Fig. 2(c).

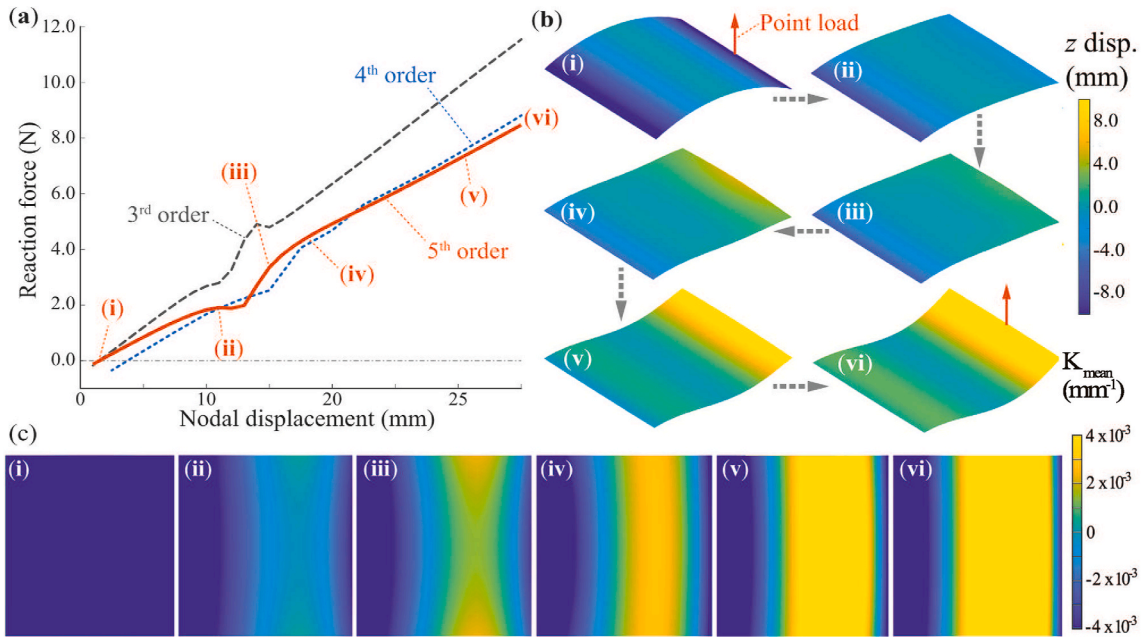

Fig. 7. Analytical prediction of the transient deformation during the snap-through when the point load is at middle of initially straight edge (Node #5). (a) The reaction force-deformation relationships based on three polynomial functions with different orders. (b) Simulated patch deformation based on the fifth order polynomial fit. (c) The mean curvature distribution based on fifth order polynomial fit.

3.3. One-step snap at node #2

The analytical model used above can reproduce the results of two-step snap and no-snap behaviors gracefully; however, it appears to fail for the one-step snap when the point load is at node #2. As observed from the FEA and experiment results (Fig. 3), there are two fronts of curvature inversion emerging from the center of the laminate. Even the fifth-order polynomial approximation of the out-of-plane displacement (10) is found incapable of capturing such complex mean curvature changes *during* the snap-through. To reproduce the results of the one-step snap-through, we would probably need a much higher-order polynomial. which would drastically increase the number of unknown constants, computation time, numerical error, and the overall analytical model's complexity. This is against our analytical study's original aim: to explore the feasibility of using the computationally inexpensive Hyer's model to qualitatively predict the different snap-through behaviors based on point load positions with reasonable accuracy.

Therefore, the extended Hyer's model with a fifth-order polynomial approximation has both success and limitations. It gives a good approximation of the transient deformation and curvature distribution

in the two-step snap-through and no snap-through scenarios. However, it fails to capture the complexity in the one-step snap-through. A critical insight from this study is that, for any reduced-order analytical model to be successful in approximating the transient snap-through behavior, it must approximate the corresponding curvature changes with reasonable accuracy.

4. Summary and conclusion

Via experimental measurements, finite element simulations, and analytical modeling, this study thoroughly examines the transient snap-through deformation of a [0°/90°] bistable composite laminate subjected to an asymmetric point load. The results show three unique types of snap-through behaviors, depending on the point load location. When the point load is on the axis defined by the middle point of the initially curved edge (Node #2) and the fixed laminate center, the laminate snap-through occurs in a single step. If the point load on a line joining the middle of the initially straight edge (Node #5) and the laminate center, snap-through never occurs regardless of the point load magnitude. For all other point load locations, the laminate snap-through occurs in two consecutive steps.

Moreover, the evolution of laminate surface curvature distribution directly correlates to the occurrence of the snap-through. As the point load increases, a localized zone of inverted curvature would initiate from the fixed center and grow towards the point load position. The different steps of snap-through occur when the curvature inversion zone reaches different edges of the bistable laminate. In particular, the snap-through completes only when the curvature inversion reaches *both* of the initially straight edges (aka. left and right edge). In the two-step snap, the curvature inversion reaches these two edges consecutively; in the one-step snap, the inversion reaches two edges simultaneously; and finally in the no-snap scenario, the inversion never reaches the left edge.

Finally, this study explores the feasibility of using an extended Hyer's model to predict the complicated snap-through behaviors qualitatively. This model uses a third, fourth, and fifth-order polynomial functions to approximate the laminate out-of-plane displacements. Using a novel way to constrain the potential function, we were able to solve the snap-through process by using quasi-static approach. The results show that, depending on the complexity of curvature inversion distribution, the extended model has a mix of success and limitation. In particular, the fifth-order polynomial approximation of the displacement field (aka. cubic curvature distribution) can satisfactorily predict the two-step snap (with some model modification) and no-snap scenarios. However, it fails to capture the complex curvature inversions in the one-step snap scenario. Predicting this one-step snap-through would require a much higher order polynomial function with a much higher computational cost.

Regardless, this study's results can offer valuable insights into the fundamental mechanics of snap-through behaviors and the actuation locations associated with the bistable composite laminates. The out-of-plane actuation used in this study has unique advantages compared to in-plane actuators, such as embedded piezoelectric patches, because the latter could hinder bistability due to their additional stiffness [39]. And this study's result could serve as a guide, allowing the user to choose the actuation force's location based on the snap-through mechanics. One could first examine the characteristics of different snap-through processes and then select the actuator's position according to its capability. For example, if the [0°/90°] patch is selected and the actuator has a high block force but low stroke (e.g., piezoelectric actuators), one can place the actuator at any point along the axis joining the Node #2 and center. This is because the corresponding snap-through involves a single step with minimal displacement requirement. On the other hand, if the actuator has a high stroke but low block force (e.g., shape memory polymers), Node #1 is the favorable actuating location as the critical force requirement is the least.

CRediT authorship contribution statement

Vishrut Deshpande: Conceptualization, Methodology, Software, Formal analysis, Investigation, Writing – original draft, Data curation, Visualization. **Oliver Myers:** Methodology, Resources, Writing – review & editing, Supervision. **Georges Fadel:** Methodology, Resources, Writing – review & editing, Supervision. **Suyi Li:** Methodology, Validation, Resources, Writing – original draft, Visualization, Project administration, Funding acquisition.

Declaration of competing interest

The authors declare that they have no known competing financial interests or personal relationships that could have appeared to influence the work reported in this paper.

Acknowledgement

The authors thank Kaitlynn Conway and Dr. Garret Pataky for assisting the setup of DIC. The authors also acknowledge the support from National Science Foundation (CMMI-1760943). S Li also acknowledge the support from Clemson University CECAS Dean's Faculty Fellowship. Gratitude is also extended to Jebin B. and Akshay B. for some useful insights.

Appendix A. Supplementary data

Supplementary data to this article can be found online at https://doi.org/10.1016/j.compscitech.2021.108871.

References

[1] C. Maurini, J. Pouget, S. Vidoli, Distributed piezoelectric actuation of a bistable buckled beam, Eur. J. Mech. Solid. 26 (2007) 837–853, https://doi.org/10.1016/j.euromechsol.2007.02.001.
[2] A. Arnaud, J. Boughaleb, S. Monfray, F. Boeuf, O. Cugat, T. Skotnicki, Thermo-mechanical efficiency of the bimetallic strip heat engine at the macro-scale and micro-scale, J. Micromech. Microeng. 25 (2015) 104003, https://doi.org/10.1088/0960-1317/25/10/104003.
[3] J. Barth, B. Krevet, M. Kohl, A bistable shape memory microswitch with high energy density, Smart Mater. Struct. 19 (2010), https://doi.org/10.1088/0964-1726/19/9/094004, 094004.
[4] W. Zhang, X. Wang, Y. Wang, G. Yang, C. Gu, W. Zheng, Y.-M. Zhang, M. Li, S.X.-A. Zhang, Bio-inspired ultra-high energy efficiency bistable electronic billboard and reader, Nat. Commun. 10 (2019) 1559, https://doi.org/10.1038/s41467-019-09556-5.
[5] D. Angeli, J.E. Ferrell Jr., E.D. Sontag, Detection of multistability, bifurcations, and hysteresis in a large class of biological positive-feedback systems, Proc. Natl. Acad. Sci. U. S. A 101 (2004) 1822–1827, https://doi.org/10.1073/pnas.0308265100.
[6] J. Elf, Spontaneous separation of bi-stable biochemical systems into spatial domains of opposite phases, Syst. Biol. 1 (6) (2004) 230–236.
[7] A. Rafsanjani, D. Pasini, Bistable auxetic mechanical metamaterials inspired by ancient geometric motifs, Extreme Mech. Lett. 9 (2016) 291–296, https://doi.org/10.1016/j.eml.2016.09.001.
[8] S. Kamrava, D. Mousanezhad, H. Ebrahimi, R. Ghosh, A. Vaziri, Origami-based cellular metamaterial with auxetic, bistable, and self-locking properties, Sci. Rep. 7 (2017) 46046, https://doi.org/10.1038/srep46046.
[9] Y. Wu, R. Chaunsali, H. Yasuda, K. Yu, J. Yang, Dial-in topological metamaterials based on bistable stewart platform, Sci. Rep. 8 (2018) 112, https://doi.org/10.1038/s41598-017-18410-x.
[10] P. Bhovad, J. Kaufmann, S. Li, Peristaltic locomotion without digital controllers: exploiting multi-stability in origami to coordinate robotic motion, Extreme Mech. Lett. 32 (2019) 100552, https://doi.org/10.1016/j.eml.2019.100552.
[11] T. Chen, O.R. Bilal, K. Shea, C. Daraio, Harnessing bistability for directional propulsion of soft, untethered robots, Proc. Natl. Acad. Sci. Unit. States Am. 115 (2018) 5698–5702, https://doi.org/10.1073/pnas.1800386115.
[12] Z. Zhang, X. Li, X. Yu, H. Chai, Y. Li, H. Wu, S. Jiang, Magnetic actuation bionic robotic gripper with bistable morphing structure, Compos. Struct. 229 (2019) 111422, https://doi.org/10.1016/j.compstruct.2019.111422.
[13] J.L. Silverberg, J.-H. Na, A.A. Evans, B. Liu, T.C. Hull, C. Santangelo, R.J. Lang, R. C. Hayward, I. Cohen, Origami structures with a critical transition to bistability arising from hidden degrees of freedom, Nat. Mater. 14 (2015) 389–393, https://doi.org/10.1038/nmat4232.
[14] H. Fang, S. Li, H. Ji, K.W. Wang, Dynamics of a bistable miura-origami structure, Phys. Rev. E 95 (2017), https://doi.org/10.1103/PhysRevE.95.052211, 052211.

[15] H. Yasuda, Z. Chen, J. Yang, Multitransformable leaf-out origami with bistable behavior, J. Mech. Robot. 8 (2016), https://doi.org/10.1115/1.4031809.
[16] R.L. Harne, K.W. Wang, A review of the recent research on vibration energy harvesting via bistable systems, Smart Mater. Struct. 22 (2013), https://doi.org/10.1088/0964-1726/22/2/023001, 023001.
[17] S.P. Pellegrini, N. Tolou, M. Schenk, J.L. Herder, Bistable vibration energy harvesters: a review, J. Intell. Mater. Syst. Struct. 24 (2013) 1303–1312, https://doi.org/10.1177/1045389X12444940.
[18] M.W. Hyer, Some observations on the cured shape of thin unsymmetric laminates, J. Compos. Mater. 15 (1981) 175–194, https://doi.org/10.1177/002199838101500207.
[19] S. Daynes, P.M. Weaver, Review of shape-morphing automobile structures: concepts and outlook, Proc. Inst. Mech. Eng. - Part D J. Automob. Eng. 227 (2013) 1603–1622, https://doi.org/10.1177/0954407013496557.
[20] S. Daynes, P.M. Weaver, A morphing trailing edge device for a wind turbine, J. Intell. Mater. Syst. Struct. 23 (2012) 691–701, https://doi.org/10.1177/1045389X12438622.
[21] J.P. Udani, A.F. Arrieta, Analytical modeling of multi-sectioned Bi-stable composites: stiffness variability and embeddability, Compos. Struct. 216 (2019) 228–239, https://doi.org/10.1016/j.compstruct.2019.02.015.
[22] Q. Ai, P.M. Weaver, T.K. Barlas, A.S. Olsen, H.A. Madsen, T.L. Andersen, Field testing of morphing flaps on a wind turbine blade using an outdoor rotating rig, Renew. Energy 133 (2019) 53–65, https://doi.org/10.1016/j.renene.2018.09.092.
[23] F. Fiorito, M. Sauchelli, D. Arroyo, M. Pesenti, M. Imperadori, G. Masera, G. Ranzi, Shape morphing solar shadings: a review, Renew. Sustain. Energy Rev. 55 (2016) 863–884, https://doi.org/10.1016/j.rser.2015.10.086.
[24] F. Dai, H. Li, S. Du, A multi-stable lattice structure and its snap-through behavior among multiple states, Compos. Struct. 97 (2013) 56–63, https://doi.org/10.1016/j.compstruct.2012.10.016.
[25] S.A. Emam, D.J. Inman, A Review on Bistable Composite Laminates for Morphing and Energy Harvesting, Applied Mechanics Reviews, 2015, https://doi.org/10.1115/1.4032037.
[26] M.-l. Dano, M.W. Hyer, Thermally-induced deformation behavior of unsymmetric laminates, Int. J. Solid Struct. 35 (1998) 2101–2120, https://doi.org/10.1016/S0020-7683(97)00167-4.
[27] K. Potter, P. Weaver, A.A. Seman, S. Shah, Phenomena in the bifurcation of unsymmetric composite plates, Compos. Appl. Sci. Manuf. 38 (2007) 100–106, https://doi.org/10.1016/j.compositesa.2006.01.017.
[28] D.N. Betts, A.I. Salo, C.R. Bowen, H.A. Kim, Characterisation and Modelling of the Cured Shapes of Arbitrary Layup Bistable Composite Laminates, Composite Structures, 2010, https://doi.org/10.1016/j.compstruct.2009.12.005.
[29] A. Pirrera, D. Avitabile, P.M. Weaver, Bistable plates for morphing structures: a refined analytical approach with high-order polynomials, Int. J. Solid Struct. 47 (2010) 3412–3425, https://doi.org/10.1016/j.ijsolstr.2010.08.019.
[30] D.V. Murray, O.J. Myers, Modeling bistable composite laminates for piezoelectric morphing structures, ISRN Mater. Sci. (2013) 1–12, https://doi.org/10.1155/2013/428624.
[31] P.F. Giddings, H.A. Kim, A.I. Salo, C.R. Bowen, Modelling of piezoelectrically actuated bistable composites, Mater. Lett. 65 (2011) 1261–1263, https://doi.org/10.1016/j.matlet.2011.01.015.
[32] P. Portela, P. Camanho, P. Weaver, I. Bond, Analysis of morphing, multi stable structures actuated by piezoelectric patches, Comput. Struct. 86 (2008) 347–356, https://doi.org/10.1016/j.compstruc.2007.01.032.
[33] F. Mattioni, P.M. Weaver, M.I. Friswell, Multistable composite plates with piecewise variation of lay-up in the planform, Int. J. Solid Struct. 46 (2009) 151–164, https://doi.org/10.1016/j.ijsolstr.2008.08.023.
[34] A. Algmuni, F. Xi, H. Alighanbari, Design and analysis of a grid patch multi-stable composite, Compos. Struct. 246 (2020) 112378, https://doi.org/10.1016/j.compstruct.2020.112378.
[35] A.S. Panesar, P.M. Weaver, Optimisation of blended bistable laminates for a morphing flap, Compos. Struct. 94 (2012) 3092–3105, https://doi.org/10.1016/j.compstruct.2012.05.007.
[36] M.L. Dano, M.W. Hyer, Snap-through of unsymmetric fiber-reinforced composite laminates, Int. J. Solid Struct. 40 (2000) 5949–5972, https://doi.org/10.1016/S0020-7683(03)00374-3.
[37] M.A. Cantera, J.M. Romera, I. Adarraga, F. Mujika, Modelling and testing of the snap-through process of bi-stable cross-ply composites, Compos. Struct. 120 (2015) 41–52, https://doi.org/10.1016/j.compstruct.2014.09.064.
[38] A. Lele, V. Deshpande, O. Myers, S. Li, Snap-through and stiffness adaptation of a multi-stable Kirigami composite module, Compos. Sci. Technol. 182 (2019) 107750, https://doi.org/10.1016/j.compscitech.2019.107750.
[39] M.-L. Dano, M. Jean-St-Laurent, A. Fecteau, Morphing of bistable composite laminates using distributed piezoelectric actuators, Smart Mater. Res. (2012) 1–8, https://doi.org/10.1155/2012/695475.